공학석사학위논문

BTX Production via Direct Dehydroaromatization of Methane and Propane over Gallium-based Zeolites

갈륨 산화물이 담지된 제올라이트 촉매상에서 메탄 및 프로판의 직접 탈수소방향족화 반응을 통한 BTX 생산

2018년 8월

서울대학교 대학원

화학생물공학부

송 창 열

Abstract

BTX Production via Direct Dehydroaromatization of Methane and Propane over Gallium-based Zeolites

Changyeol Song

School of Chemical and Biological Engineering

The Graduate School

Seoul National University

Recently, due to development of shale gas, which consists of mainly methane and light paraffin, many researches about efficient conversion of methane and light paraffin have been attempted. Among them, researches on the production of BTX, which is rapidly increasing in demand, have attracted attentions. In this work, modification of pore structure of zeolites have been studied and applied for BTX (benzene, toluene, and xylene) production by co-aromatization of methane and propane. In particular, a carbon template was introduced to conventional microporous HZSM-5 and HZSM-11 (denoted as micro-HZSM-5 and micro-HZSM-11). Mesoporous HZSM-5 and HZSM-11 (denoted as meso-

HZSM-5 and meso-HZSM-11, respectively) were synthesized to enhance the mass transfer and coke resistance of conventional zeolites. In order to activate the reactants, the same amount of gallium oxide (2 wt% with respect to each zeolite) was doped into prepared zeolites (denoted as GaO_y/micro-HZSM-5, GaO_y/micro-HZSM-11, GaO_y/meso-HZSM-5, and GaO_y/meso-HZSM-11) by using a wetness impregnation method. It was revealed that gallium oxide supported on mesoporous zeolites showed higher BTX selectivity and BTX yield than microporous zeolites with less coke deposition. Between GaO_y/meso-HZSM-5 and GaO_y/meso-HZSM-11, the effect of introduction of mesopore in meso-HZSM-11 was more significant than meso-HZSM-5. It was known that interaction between zeolites and GaO^+ species played an important role on dehydrogenation of reactant, which was a rate-determining step of dehydroaromatization process. According to XPS, H_2-TPR, and NH_3-TPD analyses, GaO_y/meso-HZSM-11 showed the stronger interaction with GaO^+ species than GaO_y/meso-HZSM-5. It was found that larger amount of GaO^+ species in GaO_y/meso-HZSM-11 was corresponding to high conversion of methane and propane.

Accordingly, a series of $XGaO_y$/meso-HZSM-11 (X = 0, 1, 2, 4, and 8) catalysts with different amount of gallium oxide loading (X, wt%) were prepared to optimize the catalytic performance. Correlation between acid properties of $XGaO_y$/meso-HZSM-11 and catalytic performance was investigated. Among tested catalysts, $1GaO_y$/meso-HZSM-11 exhibited the best catalytic performance with the largest amount of acidity. Also, $4GaO_y$/meso-HZSM-11 and $8GaO_y$/meso-HZSM-11 showed severe deactivation over times while less amount of gallium loading supported catalysts showed stable catalytic performance. Therefore, an optimum amount of gallium loading is required for improving

BTX production by co-aromatization of methane and propane.

Keywords : BTX production, Gallium oxide, mesoporous HZSM-5, mesoporous HZSM-11, Coaromatization, Dehydroaromatization, Methane, Propane

Student Number : 2016-25837

Contents

List of Figures

List of Tables

1. Introduction

Among petrochemical industries, aromatics manufacturing industries such as, benzene, toluene, and xylene (BTX) are nationally attracting more attentions. With the rapid increasing demand of BTX, which are basic raw materials for producing PET, polyester, polystyrene, etc., new technology for promoting the production of BTX is required. [1]

Since BTX has been manufactured on the basis of naphtha, which is extracted from crude oil, production of BTX is unstable due to long-term imbalance in supply of crude oil and a sharp change in price. In order to avoid dependence on crude oil, renewable energies are considered as alternative resource of petrochemical industry due to crude oil on the brink of being exhausted. In particular, abundant methane has been being produced due to increase in shale gas. Since methane is one of the most plentiful renewable energy as a main constituent of shale and natural gas, the application of methane as a feedstock is crucial for various chemical reactions and it has infinite possibilities for production of high-value compounds. For these reason, many researches have been performed on direct dehydroaromatization of methane to produce aromatic compounds because BTX (benzene, toluene, and xylenes) are raw materials for high-value compounds such as PET, polyester, and polystyrene. Nevertheless, direct conversion of methane has a difficulty in producing aromatic compounds because high temperature is required for endothermic reaction. Activation of CH_4 molecules to intermediates is rate-determining step for dehydroaromatization due to high activation barrier of C-H bond. Therefore, light paraffin such as propane is introduced as a co-feedstock to lower the thermodynamic

limitation. Activation of C-H bond in the presence of propane becomes easier as expected by the thermodynamic parameters of aromatization reactions. In other words, Co-aromatization of methane and propane is more efficient process for BTX production than direct conversion of methane to BTX. [2, 3]

The widely studied catalysts for co-aromatization are transition metal oxide supported on zeolites because dehydroaromatization reaction requires dual active sites of the bi-functional catalyst for BTX production. A reaction mechanism of co-aromatization is summarized as follows. Transition metal oxide sites activate reactants to produce ethylene and propylene as intermediates, and then acid sites of the catalysts advance cyclization of intermediates to BTX.

Among several transition metal oxides such as Ga, Zn, Mo, Fe, and Ni, Zn and Ga oxides have been mainly used for metal active sites because Zn and Ga modified zeolites catalysts show outstanding catalytic performance compared to other metal oxides modified zeolites [4, 5]. Since Zn and Ga metal modified zeolites have excellent ability to exchange electrons due to high electron capacity for methane and propane activation, Zn and Ga have been most dominantly introduced to dehydroarmatization reaction in recent researches. However, Zn-doped zeolites exhibited rapid deactivation of the catalysts with poor stability. Instead, Ga-containing ZSM-5 zeolites recently have attracted attentions for dehydroaromatization of light paraffin due to its synergetic effects with zeolites [5-10]. Incorporation of Ga with zeolites enhances formation of stronger Lewis acid sites. Also, extra-framework gallium species $(GaO)^+$ reduce the rate-determining dehydrogenation step of dehydroaromatization reaction.

In order to create mesoporosity within zeolite crystals, dealumination or

desilication of conventional zeolites were performed. Organic hydroxide or NaOH leaching has been widely used to extract silicon of the zeolite framework. The mesopores were formed at the site where silicon was extracted. Also, J. Zhou et al. [11-13] revealed that block-copolymer could be used as a scaffold with assistance of pre-steaming treatment. As a result, coke formation was inhibited and mass transfer was enhanced due to shortened diffusion path in micropore network.

In present work, a carbon template (BP-2000) was introduced into conventional zeolites during crystallization process under hydrothermal treatment to improve pore structure of ZSM-11 and ZSM-5. By combustion of the carbon after crystallization, mesopores were formed at the site where the carbon templates were combusted. In order to compare the catalytic performance of ZSM-5 and ZSM-11, gallium oxide supported mesoporous HZSM-5 and HZSM-11 were synthesized. Textural properties of both mesoporous HZSM-5 and HZSM-11 were investigated by N_2 adsorption-desorption, XRD, and SEM. In addition, XPS, ^{27}Al NMR, H_2-TPR, and NH_3-TPD were performed to elucidate chemical properties of the prepared mesoporous zeolites.

2. Theory and background

2.1. Methane and propane dehydroaromatization

Dehydroarmoatization reaction of light paraffin is endothermic reaction. Since bonding energy of C-C is approximately 246 kJ/mol which is less than C-H bonding energy of 363 kJ/mol, dehydrogenation requires more energy than cracking of hydrocarbons. In recent years, many researches about methane dehydroaromatization (MDA) have been attempted due to increase in production of methane. Because dehydroaromatization is an endothermic reaction, high temperature conditions are required in the process. Therefore, various methods are being tried to avoid the deactivation of the catalysts due to the deposition of carbon during the reaction. In present work, a small amount of light paraffin was added to lower the thermodynamic restriction. With addition of a small amount of propane, the thermodynamic limit can be lowered and the reaction temperature also can be reduced, leading more energy-efficient process design. Detailed thermodynamic constants are shown below [14].

$6CH_4(g) \rightarrow C_6H_6(g) + 9H_2(g)$ $\quad \Delta H_r^\circ = 532.2$ kJ/mol

$2C_3H_8 \rightarrow C_6H_6 + 5H_2$ $\quad \Delta H_r^\circ = 290.6$ kJ/mol

$CH_4+2C_3H_8 \rightarrow C_6H_5CH_3+6H_2$ $\quad \Delta H_r^\circ = 332.6$ kJ/mol

Among reactions shown, coaromatzation of methane and propane shows the lowest energy limit compared to formation of benzene from only methane or propane, indicating

dehydroaromatization of the reaction can be operated at the modest condition. Even though a small amount of propane is added, intermediate from propane also activate methane to form another intermediate such as carbenium ion. In dehydroaromatization of light paraffin, it is known that both Lewis acid site and Brönsted-Lowry acid site play important roles. Light paraffins are activated by hydrogen transfer at Lewis acid site. The produced intermediates are oligomerized or cyclized at Brönsted-Lowry acid site on zeolites. Accordingly, the most appropriate ratio of Lewis acid and Brönsted-Lowry acid is required for optimizing the dehydroaromatization reaction. Proposed mechanism is shown in Fig 2.1.1. Lewis acid site of catalysts are formed by transition metal oxides and Brönsted-Lowry acid site is formed by zeolites. Therefore, as amount of transition metal loading increases, the amount of Lewis acid site also increases. As mentioned above, it was known dehydrogenation of light paraffin occurs at Lewis acid site. To be more specific, the interaction between zeolites and highly dispersed Ga (GaO^+ species) is responsible for hydrogen transfer. It can be said interaction between zeolites and highly dispersed gallium (GaO^+ species) is closely related to conversion rate of reactants since reactants can start converting into other chemicals with dehydrogenation.

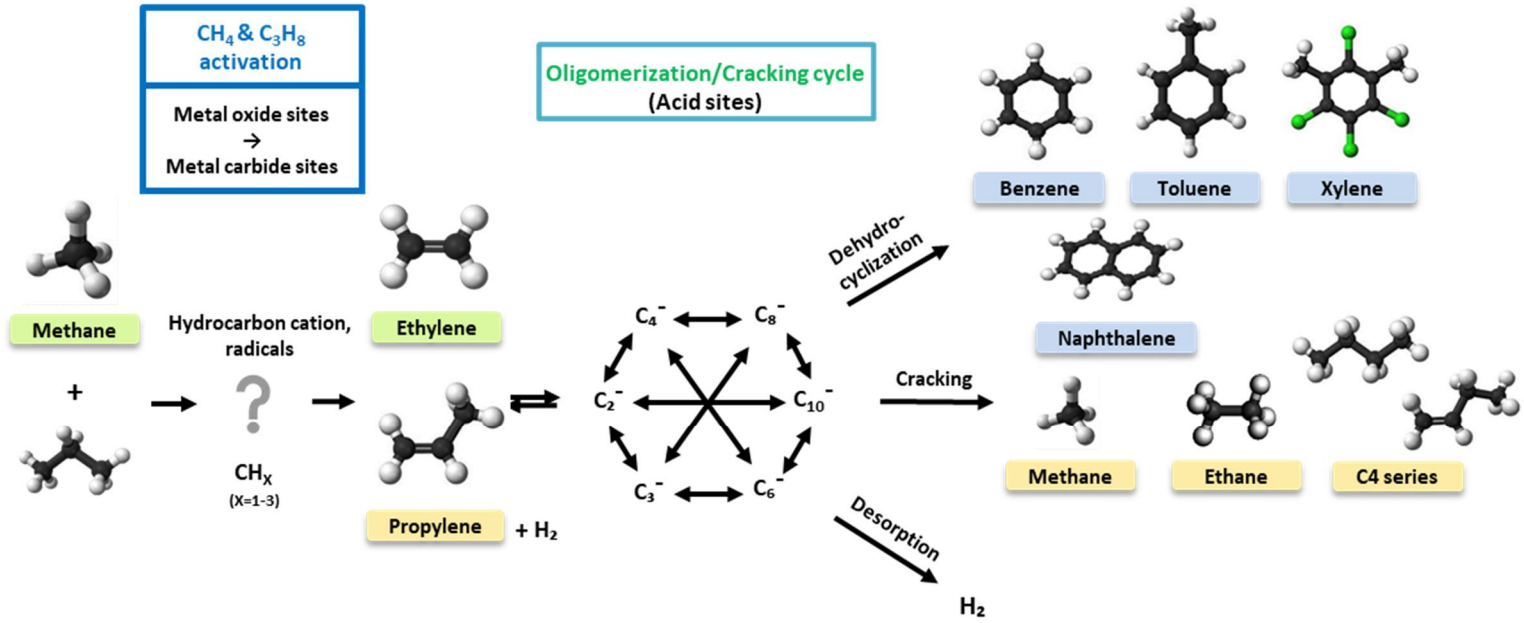

Fig. 2.1.1. Proposed mechanism for dehydroaromatization of methane and propane.

2.2. Introduction of mesopores into ZSM-5 and ZSM-11

Among zeolites tested for dehydroaromatization reactions, ZSM-5 and ZSM-11 have been studied extensively for many petrochemicals due to their unique structure [15]. Both zeolites have similar framework and pore size, but they are different in channel structure as shown in Fig 2.2.1. ZSM-11 only consists of straight channel while ZSM-5 has both straight and sinusoidal channels. It was reported ZSM-11 has less diffusion resistance than ZSM-5 because of their different channels. It was also revealed advantageous channel structure of ZSM-11 can be enhanced by adopting mesopores in the zeolites. Thereby many attempts have been made to modify the pore structure of conventional zeolites in various methods [16].

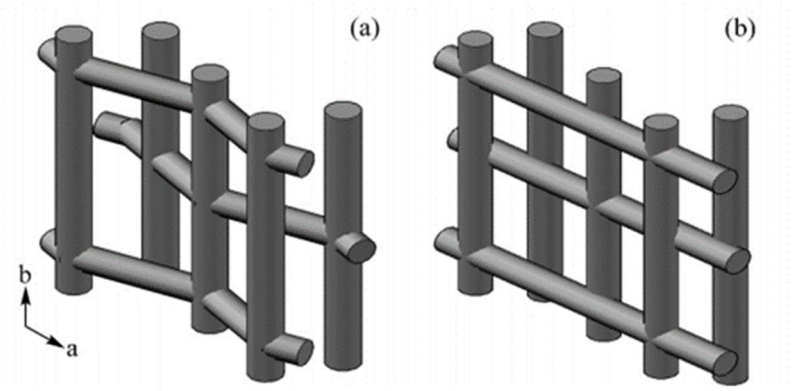

Fig. 2.2.1. Channel structure of ZSM-5 (a) and ZSM-11 (b)

3. Experiments

3.1. Preparation of catalysts

3.1.1. Materials

Raw materials used for zeolite synthesis are sodium hydroxide (NaOH, 98.0%, Samchun Chemical), sodium aluminate ($NaAlO_2$, Na_2O 35.0%, Al_2O_3 52.0%, Junsei), tetraethyl orthosilicate (TEOS, 98%, reagent grade, Sigma Aldrich), tetrapropylammonium bromide (TPABr, 98%, Sigma Aldrich), tetrabutylammonium bromide (TBABr, 99%, Samchun Chemical), carbon template (BP-2000, Carbot Corp.), ammonium nitrate (NH_4NO_3, 99%, Junsei) and deionized water. Gallium (III) nitrate hydrate (99.0% Alfa Aesar) was also used as a precursor.

3.1.2. Preparation of mesoporous HZSM-5 and HZSM-11

In this research, hard templating method was introduced to improve pore structure of conventional HZSM-5 and HZSM-11. The composition of the reaction mixture was fixed as $1Si:0.033Al:0.07Na_2O:0.03template:35H_2O$ where templates are TPABr for HZSM-5 and TBABr for HZSM-11. The procedure for mesoporous HZSM-5 and HZSM-11 synthesis is as follow. First of all, 1.30 g of NaOH was dissolved in 108 ml of deionized water at room temperature. 0.47 g of $NaAlO_2$ and 1.36 g of template (TPABr or TBABr) were dissolved in the NaOH solution with vigorous stirring for 1 hour. And then, 38.2 ml of tetraethyl orthosilicate was added into the clear solution of mixtures with vigorous

stirring as well. After 3 hours, 1 weight percent of BP-2000 carbon template with respect to Si and Al sources was added into the solution of mixtures and the mixture was stirred for another 3 hours. The mixtures were introduced to a teflon-lined autoclave for crystallization under hydrothermal treatment. The hydrothermal synthesis was operated at 160 °C for 72 hours under autogenous pressure. The products, after crystallization, were filtered and washed with 1 liter of deionized water three times. The filtered products were then dried at 110 °C in an oven overnight. Dried products were calcined in an air atmosphere at 550 °C for 10 hours to get rid of carbon template and organics. Mesopores of zeolites are formed at the site where carbon template was removed in this process. For ion-exchange of Na^+-form ZSM-5 and ZSM-11 to NH_4^+-form, the zeolites were added in 1 M solution of ammonium nitrate at 100 °C for 3 hours. This process was repeated three times for complete ion-exchange and followed by washing and drying to obtain the NH_4^+-form zeolites. Finally, the ion-exchanged zeolites were calcined at 550 °C for 5 h to obtain H-form mesoporous ZSM-5 (meso-HZSM-5) and H-form mesoporous ZSM-11 (meso-HZSM-11).

3.1.3. Preparation of conventional (microporous) HZSM-5 and HZSM-11

Conventional HZSM-5 (micro-HZSM-5) and HZSM-11 (micro-HZSM-11) were synthesized as well. The synthesis process for both conventional HZSM-5 and HZSM-11 was the same as the process of synthesizing mesoporous zeolites except for the introduction of carbon template (BP-2000) during crystallization.

3.1.4. Preparation of gallium oxides supported on zeolites

Gallium oxides supported on zeolites were prepared by using wet impregnation method. 1 g of prepared zeolites was added into a 10 ml of deionized water for wetness impregnation at 75 °C. A calculated amount of gallium (III) nitrate hydrate was then dissolved into the aqueous solution. After impregnation, gallium oxides supported on mesoporous zeolites (HZSM-5 and HZSM-11) and microporous zeolites with same amount of gallium loading (2 wt% with respect to zeoiltes) were prepared. The gallium oxides supported on zeolites were denoted as GaO_y/meso-HZSM-5, GaO_y/meso-HZSM-11, GaO_y/micro-HZSM-5, and GaO_y/micro-HZSM-11 respectively.

In addition, various amount of gallium loading was impregnated into meso-HZSM-11 for optimizing acid property of the catalysts. $XGaO_y$/meso-HZSM-11 (X = 0, 1, 2, 4, 8) was prepared by using the same method above except for amount of gallium loading.

3.2. Characterization

3.2.1. XRD (X-Ray Diffraction)

X-ray patterns with crystalline phases of the catalysts were investigated by XRD measurements (Rigaku, D-MAX2500-PC) using Cu-Kα radiation (λ = 1.54056 Å) operated at 50 kV and 100 mA.

3.2.2. N_2 adsorption-desorption measurement

Nitrogen adsorption-desorption isotherms were acquired with a BELSORP-mini II (BEL Japan) device. Prior to the nitrogen adsorption, all the catalysts were evacuated at 200 ^{o}C for 4 h to eliminate any impurities on the catalyst surface. Surface areas of the catalysts were calculated using the BET (Brunauer-Emmett-Teller) equation. Pore volumes were determined by t-plot and the BJH (Barret-Joyner-Hallender) method applied to the desorption branch of the isotherms.

3.2.3. NH_3-TPD (temperature-programmed desorption)

NH_3-TPD (temperature-programmed desorption) experiments were carried out to determine the acid properties of the catalysts. 0.03 g of each catalyst charged into the TPD apparatus was pretreated at 200 °C for 2 h with a stream of helium (50 ml/min). After cooling the catalyst to room temperature, ammonia (50 ml/min) was introduced into the reactor at 50 °C for 30 min to saturate acid sites of the catalyst. Physisorbed ammonia was removed at 110 °C for 1 h under a flow of helium (50 ml/min). After cooling down

the sample, furnace temperature was increased from 50 °C to 500 °C at a heating rate of 5 °C/min under a flow of helium (30 ml/min). Desorbed species were detected using a BELCAT (BEL Japan Inc.) connected to a thermal conductivity detector (TCD).

3.2.4. SEM (Scanning Electron Microscopy)

The morphology of prepared catalysts was investigated by using field emission scanning electron microscopy (FE-SEM), MERLIN Compact.

3.2.5. ^{27}Al MAS NMR (Magic Angle Spinning Nuclear Magnetic Resonance)

^{27}Al MAS NMR measurements were performed using a 500 MHz solid NMR system (Bruker, Bruker AVANCE II). The ^{27}Al MAS NMR spectra were obtained by a single pulse and the Al chemical shifts were referneced to $Al(NO_3)_3$.

3.2.6. XPS (X-ray Photoelectron Spectroscopy)

X-ray photoelectron spectroscopy (XPS) analyses (K-alpha, Thermo Scientific Inc.,) were carried out to measure the binding energies of gallium (Ga $2p_{3/2}$) on surface of the catalysts. X-ray source was monochromated Al X-ray sources with Al Kα line of 1486.6 eV. XPS analysis was operated at 12 kV and 3 mA. The binding energy values were corrected for charging effect by referring to the adventitious C 1s line at 284.5 eV.

3.2.7. H_2-TPR (temperature-programmed reduction)

H_2-TPR was performed with 0.03 g of the catalyst using BEL-CAT II (BEL Japan Inc.) instrument equipped with thermal conductivity detector (TCD). The samples were pretreated in a flow of 5% H_2/Ar at 100 °C for 1 h to remove contaminants prior to the analysis. Afterwards, the sample was cooled down to room temperature and temperature was raised from room temperature to 900 °C at a rate of 10 °C/min with 30 sccm of of 5% H_2/Ar.

3.3. Direct dehydroaromatization of methane and propane

3.3.1. Reaction system of coaromatization

In this work, reaction system of coaromatization of methane and propane is shown in Fig 3.3.1. Coaromatization of methane and propane was performed in a continuous flow fixed-bed quartz reactor at 550 °C under atmospheric pressure. 0.2 g of each catalyst was charged into the quartz reactor. For coaromatization of methane and propane, volume ratio of reactants was fixed at CH_4:C_3H_8:N_2 = 5:0.5:7.5 and total GHSV was fixed at 3900 ml/h·g_{cat}. Inlet and outlet line were heated at 250 °C in order to prevent liquefaction of product. Produced molecules through catalytic reaction were periodically inserted and analyzed using an on-line gas chromatograph (YL-6100, Younglin) equipped with a GS-gaspro capillary column for a flame ionization detector (FID) and a Carboxen-1000 packed column for a thermal conductivity detector (TCD). Conversion of methane and propane and selectivity for BTX were calculated on the basis of carbon balance as

follows. BTX yield was calculated by multiplying conversion of reactants and selectivity for BTX. Note that x_i in equation (2) represents the stoichiometric coefficient of various carbon-containing products.

$$Conversion\ of\ reactants\ (\%) = \frac{Moles\ of\ reactants\ reacted}{Moles\ of\ reactants\ supplied} \times 100 \quad (1)$$

$$Selectivity\ for\ BTX\ (\%) = \frac{Moles\ of\ BTX\ \ produced \times x_i}{Moles\ of\ reactants\ reacted} \times 100 \quad (2)$$

$$BTX\ yield\ (\%) = \frac{Conversion\ of\ reactants \times Selectivity\ for\ BTX}{100} \quad (3)$$

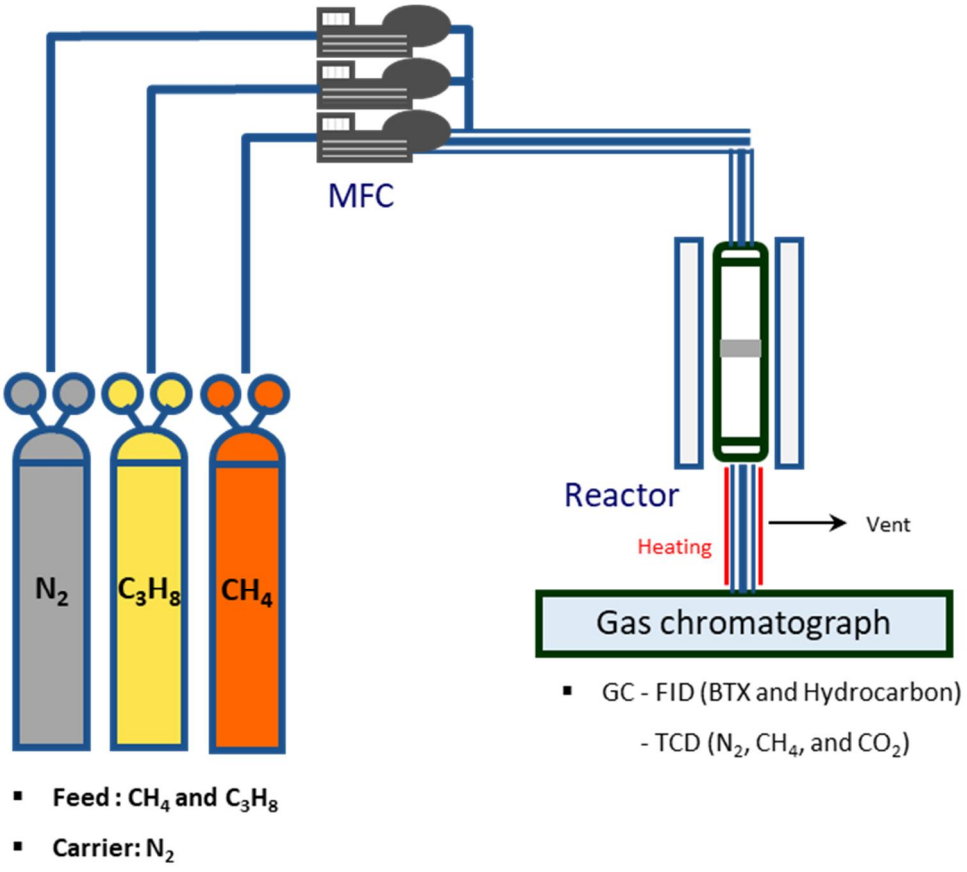

Fig 3.3.1. Scheme for the direct dehydroaromatization reactor system

4. Result and discussion

4.1. Textural properties of micro-HZSM-5, micro-HZSM-11, meso-HZSM-5 and meso-HZSM-11

In order to confirm crystal phase of micro-HZSM-5, micro-HZSM-11, meso-HZSM-5 and meso-HZSM-11, XRD analysis was performed as shown in Fig 4.1.1. The XRD patterns showed different crystalline structure of ZSM-5 and ZSM-11 between 2θ range of 23° and 25°. As ZSM-5 zeolites have five distinctive diffraction peaks representing [501], [051], [151], [303] and [133] crystal plane, ZSM-11 zeolites only have [501] and [303] peaks as shown in Fig 4.1.1 [15]. These XRD patterns also indicate both ZSM-5 and ZSM-11 were synthesized with high crystallinity. In addition, the crystallinity of the zeolites was also well-maintained without destruction of crystalline structure when carbon templates were added to synthesis procedure of zeolites.

As shown in Fig. 4.1.2, textural properties of micro-HZSM-5, micro-HZSM-11, meso-HZSM-5, and meso-HZSM-11 were investigated by nitrogen adsorption-desorption isotherm. The isotherms of both micro-HZSM-5 and micro-HZSM-11 showed type-I with the specific surface areas evaluated by BET method of 335.1 and 328.6 m^2/g, respectively. In accordance with the isotherms, formation of mesopores was not detected in case of microporous zeolites (conventional zeolites). Moreover, the isotherms of both meso-HZSM-5 and meso-HZSM-11 exhibited type-IV hysteresis loop indicating the formation of mesopores in zeolites. In consequence, mesoporous zeolites were successfully prepared. All calculated surface area and pore volume are listed in Table 4.1.1.

^{27}Al MAS NMR measurements were conducted to investigate the different environment of Al atom. As shown in Fig. 4.1.3, four-coordinate framework Al and octahedral extra-framework Al were detected at around 54 ppm and 0 ppm respectively [5, 7, 17]. It is noteworthy that a peak for octahedral extra-framework Al was observed in NMR spectra of meso-HZSM-11 while the peak was not detected in spectra of micro-HZSM-11. It can be confirmed that introducing carbon templates to form mesopores caused dealumination of frameworks in zeolites.

From SEM images (Fig. 4.1.4), structure properties of meso-HZSM-5 and meso-HZSM-11 were investigated. Cubic units of ZSM-5 sample were shown in Fig. 4.1.4 (a) while aggregation of elliptical-shaped crystalline was shown in ZSM-11 sample. Average crystal sizes were also measured by SEM micrographs, where crystal size of ZSM-5 was measured as 1.7-2.0 μm and ZSM-11 as 0.4-0.6 μm. The zeolites that have larger crystal sizes tend to form longer channels as well as longer the intracrystalline diffusion path length. In previous literature, it was reported that the effects of crystal sizes were significant as well as total acid amount of the zeolites in cracking and aromatization ability.

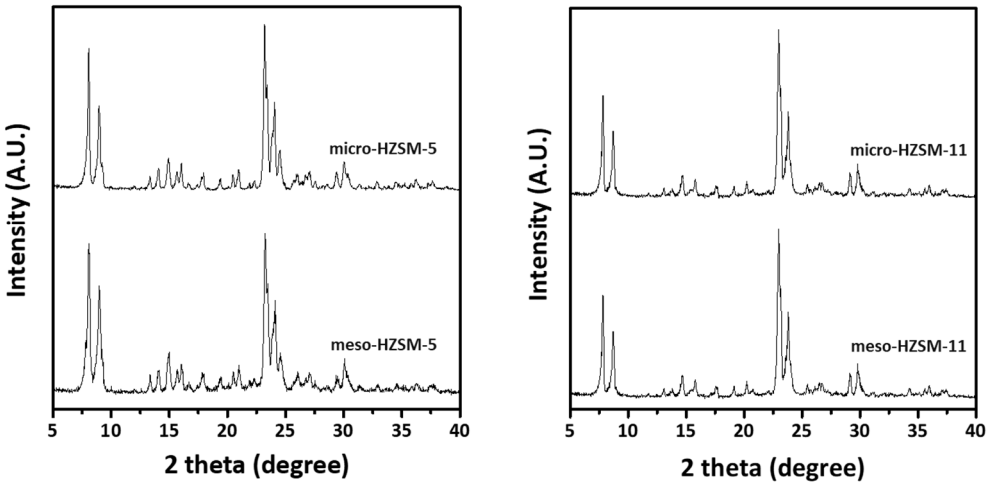

Fig. 4.1.1. XRD patterns of micro-HZSM-5, meso-HZSM-5, micro-HZSM-11 and meso-HZSM-11.

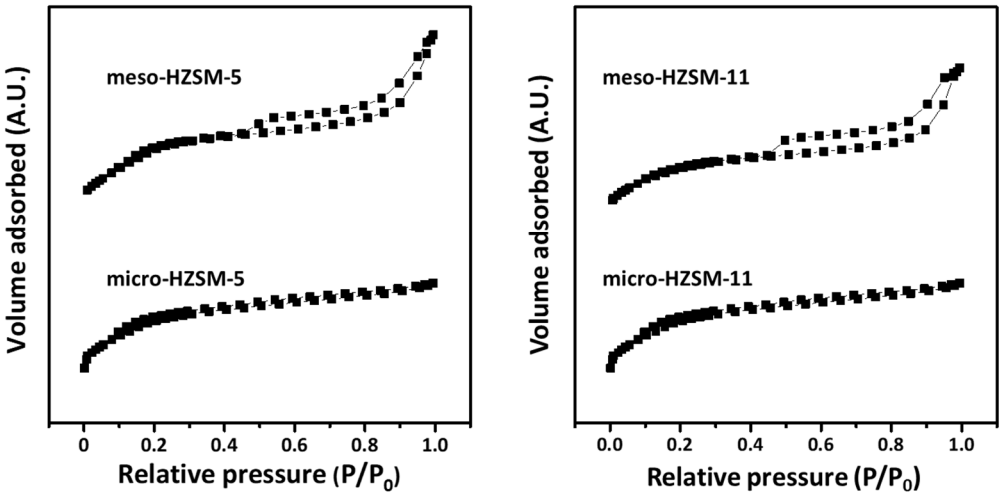

Fig. 4.1.2. Nitrogen adsorption-desorption isotherms of micro-HZSM-5, meso-HZSM-5, micro-HZSM-11 and meso-HZSM-11.

Table 4.1.1. Physicochemical properties of micro-HZSM-5, meso-HZSM-5, micro-HZSM-11, and meso-HZSM-11

Catalyst	Surface area (m^2/g)[a]	Pore volume (cm^3/g)	
		Micropore[b]	Mesopore[c]
meso-HZSM-5	347.3	0.174	0.092
micro-HZSM-5	335.1	0.196	-
meso-HZSM-11	342.9	0.167	0.099
micro-HZSM-11	328.6	0.187	-

[a] Calculated by the BET (Brunauer-Emmett-Teller) equation

[b] Determined by t-plot

[c] BJH (Barret-Joyner-Hallender) desortption pore volume

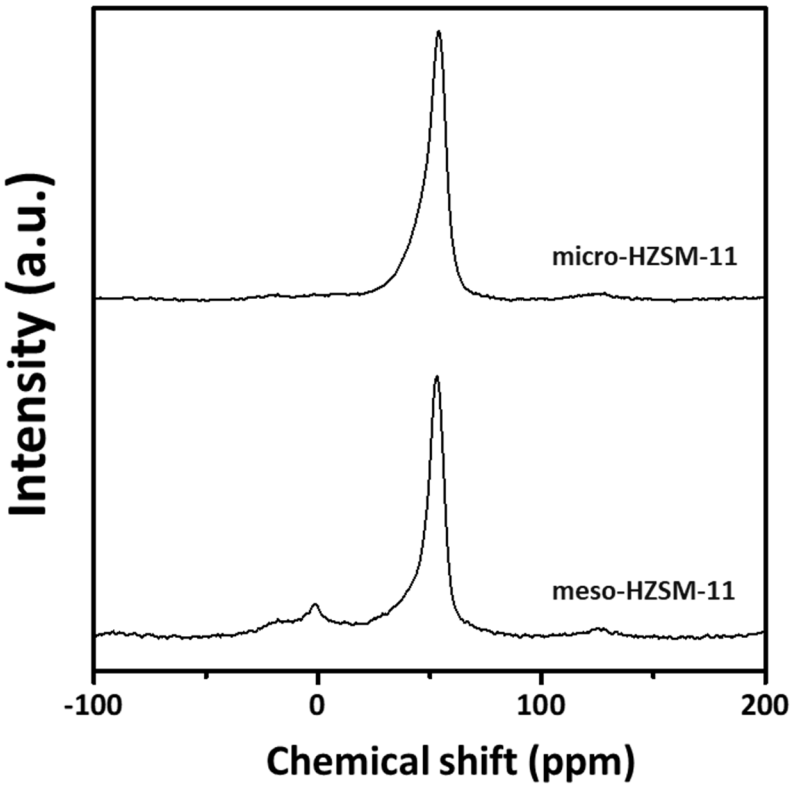

Fig. 4.1.3. ^{27}Al MAS NMR spectra of micro-HZSM-11 and meso-HZSM-11.

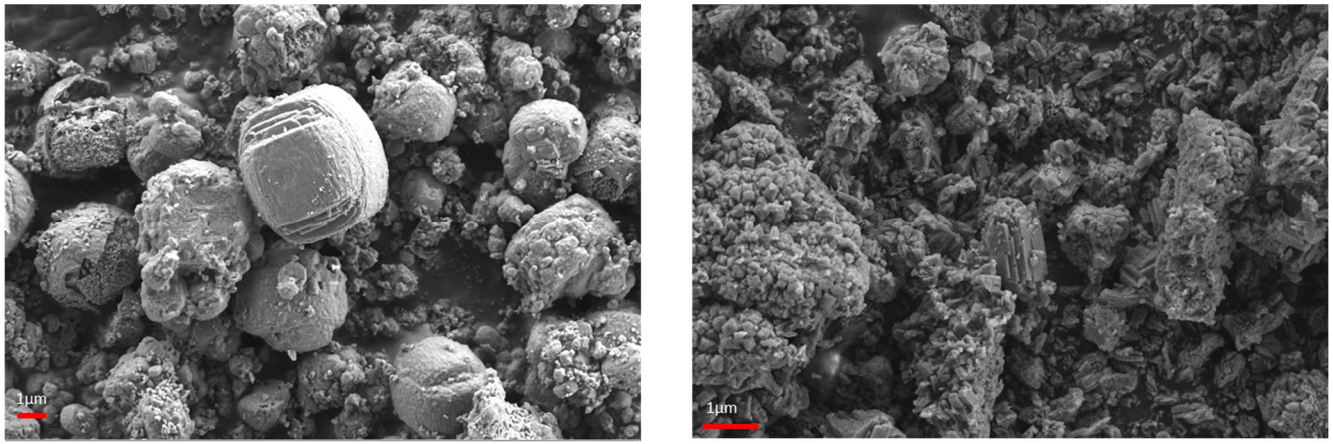

(a) **(b)**

Fig. 4.1.4. SEM images of (a) meso-HZSM-5 and (b) meso-HZSM-11.

4.2. Gallium-doped microporous and mesoporous zeolites

4.2.1. Textural properties of GaO_y/micro-HZSM-5, GaO_y/micro-HZSM-11, GaO_y/meso-HZSM-5 and GaO_y/meso-HZSM-11

X-ray diffraction (XRD) measurement was performed to investigate the crystalline structures of gallium oxide supported microporous and mesoporous zeolites as shown in Fig.4.2.1. The XRD patterns showed different crystalline structure of ZSM-5 and ZSM-11 between 2θ range of 23° and 25° as mentioned before. These XRD patterns also indicate both ZSM-5 and ZSM-11 were synthesized with high crystallinity. In addition, the crystallinity of the zeolites was also well-maintained without destruction of crystalline structure when gallium metal was added into prepared zeolites. Yellow dots in Fig 4.2.1 represents diffraction peaks for gallium oxide; however, distinct gallium oxide peaks were not shown in prepared gallium oxide supported catalysts meaning that gallium oxides were well-dispersed.

As shown in Fig. 4.2.2, textural properties of GaO_y/micro-HZSM-5, GaO_y/micro-HZSM-11, GaO_y/meso-HZSM-5, and GaO_y/meso-HZSM-11 were investigated by nitrogen adsorption-desorption isotherm. The isotherms of both GaO_y/micro-HZSM-5 and GaO_y/micro-HZSM-11 showed type-I with the specific surface. In accordance with the isotherms, formation of mesopores was not detected in case of microporous zeolites (conventional zeolites) regardless of a wetness impregnation. Moreover, the isotherms of both GaO_y/meso-HZSM-5 and GaO_y/meso-HZSM-11 exhibited type-IV hysteresis loop

indicating the maintenance of mesopores in zeolites. In consequence, surface area of gallium-doped mesoporous zeolites was slightly deceased due to addition of gallium. All calculated surface area and pore volume are listed in Table 4.2.1.

4.2.2. Catalytic performance of gallium-doped zeolites

Catalytic performance and conversions of reactants over prepared catalysts were shown in Fig 4.2.3. To be more specific, initial conversion of methane and propane, selectivity to by-product and BTX are listed in Table 4.2.2 (after 45 min. reaction). Conversion and selectivity data after 5 h reaction were also listed in Table 4.2.3 for comparison with initial catalytic performance. It was notable that gallium-doped mesoporous zeolites showed better performance than gallium-doped microporous zeolites with less deactivation of catalysts. Between GaO_y/meso-HZSM-5 and GaO_y/meso-HZSM-11, GaO_y/meso-HZSM-5 showed higher conversion rate of methane and BTX selectivity. Accordingly, BTX yield over GaO_y/meso-HZSM-5 was greater than GaO_y/meso-HZSM-11. It was also found that gallium-doped microporous zeolites showed reduced total carbon over reaction while gallium-doped mesoporous zeolites maintained a certain amount of carbon according to carbon balance listed in Table 4.2.2 and Table 4.2.3. In other words, coke deposition of microporous zeolites was more preferable than mesoporous zeolites.

Surprisingly, introduction of mesopore into two different zeolites caused different results. It was observed that GaO_y/meso-HZSM-11 exhibited better performance than

GaO_y/meso-HZSM-5. Induction period of meso-HZSM-5 was detected whereas induction time of meso-HZSM-11 was not. It was assumed that induction period of ZSM-11 was shorter due to its low diffusion resistance and high mass transfer rate. In addition, only slight change in methane conversion was observed while the difference in propane conversion between GaO_y/meso-HZSM-5 and GaO_y/meso-HZSM-11 was noticeable. In order to explain better catalytic performance over GaO_y/meso-HZSM-11, H_2-TPR and XPS analyses were performed.

4.2.3. Interaction between gallium and mesoporous zeolites and reduction properties

Higher conversion of propane in GaO_y/meso-HZSM-11 can be elucidated with stronger interaction between extra-framework GaO^+ species and meso-HZSM-11 [14, 18]. It is known highly dispersed $(GaO)^+$ is an active site for hydrogen transfer, which is a rate-determining step of dehydroaromatization [7]. H_2-TPR analysis was performed to investigate the interaction between gallium metal and catalysts and reduction behavior of catalysts as shown in Fig 4.2.4. In general, gallium-doped zeolites show two different reduction peak approximately at 550~650 °C and 700~750 °C, respectively. It is known that the first peak appeared at 550~650 °C represents reduction of Ga_2O_3 to Ga_2O. Second peak appeared represents reduction of $(GaO)^+$ to Ga^+ [19]. As shown in Fig 4.2.4, reduction

temperature of second peak in GaO_y/meso-HZSM-11 is greater than GaO_y/meso-HZSM-5 indicating that interaction between GaO^+ species and GaO_y/meso-HZSM-11 was stronger. Also, larger amount of strong Lewis acid site in GaO_y/meso-HZSM-11 was expected due to larger amount of GaO^+ species. [10, 19]

XPS analyses were performed to clarify the chemical state of the elements on the surface of GaO_y/meso-HZSM-5 and GaO_y/meso-HZSM-11. In particular, Ga $2p_{3/2}$ XPS spectra enabled to elucidate the state of gallium on the surface of Ga-doped zeolites as shown in Fig. 4.2.5. Ga $2p_{3/2}$ binding energy of Ga_2O_3 was shown at approximately 1117.9 eV in the given operation condition [20]. It can be seen that Ga $2p_{3/2}$ binding energy of GaO_y/meso-HZSM-5 (1118.4 eV) and GaO_y/meso-HZSM-11 (1118.8 eV) were higher than that of Ga_2O_3 implying the interaction between the zeolites and an ionized gallium was stronger. More specifically, higher Ga $2p_{3/2}$ binding energy indicates the stronger covalent bonding between the highly dispersed Ga species (GaO^+) and the framework of the zeolites. It was observed that meso-HZSM-11 interacted covalently stronger with highly dispersed GaO^+ than meso-HZSM-5. In short, formation of highly dispersed $(GaO)^+$ was more preferred in meso-HZSM-11 compared to meso-HZSM-5 even though the same amount of gallium was loaded.

4.2.4. Acidic properties of GaO_y/meso-HZSM-5 and GaO_y/meso-HZSM-11

The acidic properties of GaO_y/meso-HZSM-5 and GaO_y/meso-HZSM-11 were investigated by NH_3-TPD measurement as shown in Fig. 4.2.6. All calculated acidity is

listed in Table 4.2.4. Three peaks of NH_3 desorption for both meso-HZSM-5 and meso-HZSM-11 appeared at different temperatures associated with weak, medium, and strong acid site, respectively. The weak acid site is due to NH_3 species desorbed in the non-exchangeable cationic site of zeolite framework. Medium acid site is mainly related to the interaction of extra-framework GaO^+ species with the acidic protons of the zeolite framework. Medium acid site is of strong Lewis acid site [20]. Strong acid site (Brönsted-Lowry acid site) is influenced by exchangeable protonic site of the zeolite framework. It was detected that desorption peaks in GaO_y/meso-HZSM-11 were shifted to higher temperature compared to that of GaO_y/meso-HZSM-5. This result means that overall acidic strength of GaO_y/meso-HZSM-11 was stronger than that of GaO_y/meso-HZSM-5. Of all acid sites, the biggest difference shown was the amount of strong Lewis acid site. It was revealed the correlation between the amount GaO^+ and the amount of Lewis acid. From the correlation, the amount of strong Lewis acid increased as the amount of GaO^+ increased. Not only the amount, but strength of Lewis acid is also an important factor. The strength of strong Lewis acid was improved due to strong interaction of the GaO^+ with the negative potential of the zeolite framework. According to XPS analysis, it was confirmed interaction between highly dispersed extra-framework GaO^+ species and meso-HZSM-11 was stronger than meso-HZSM-5.

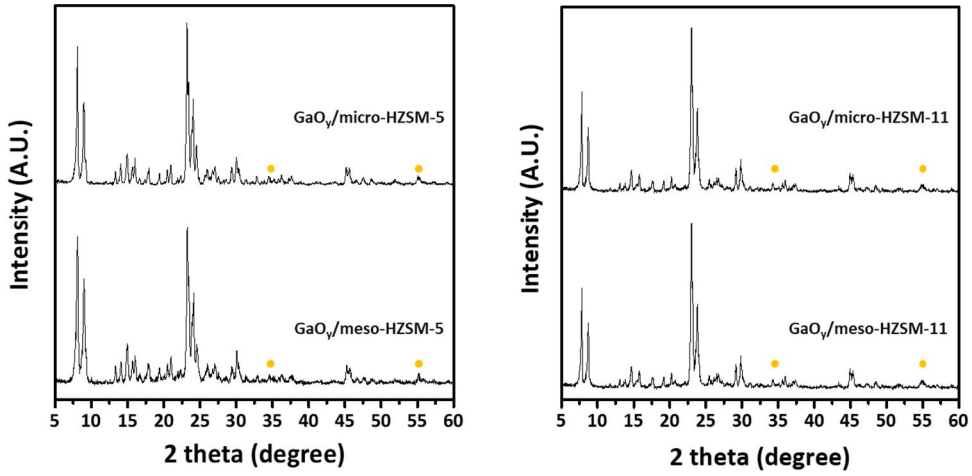

Fig. 4.2.1. XRD patterns of gallium-doped zeolites

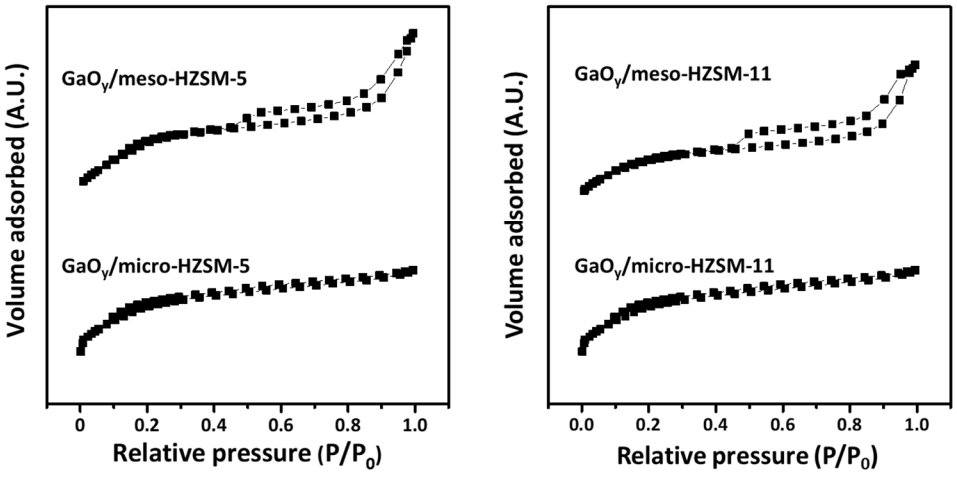

Fig. 4.2.2. Nitrogen adsorption-desorption isotherms of gallium-doped zeolites

Table 4.2.1. Physicochemical properties of GaO_y/micro-HZSM-5, GaO_y/meso-HZSM-5, GaO_y/micro-HZSM-11, and GaO_y/meso-HZSM-11

Catalyst	Surface area (m^2/g)[a]	Pore volume (cm^3/g)	
		Micropore[b]	Mesopore[c]
meso-HZSM-5	347.3	0.174	0.092
micro-HZSM-5	335.1	0.196	-
meso-HZSM-11	342.9	0.167	0.099
micro-HZSM-11	328.6	0.187	-

[a] Calculated by the BET (Brunauer-Emmett-Teller) equation

[b] Determined by t-plot

[c] BJH (Barret-Joyner-Hallender) desorption pore volume

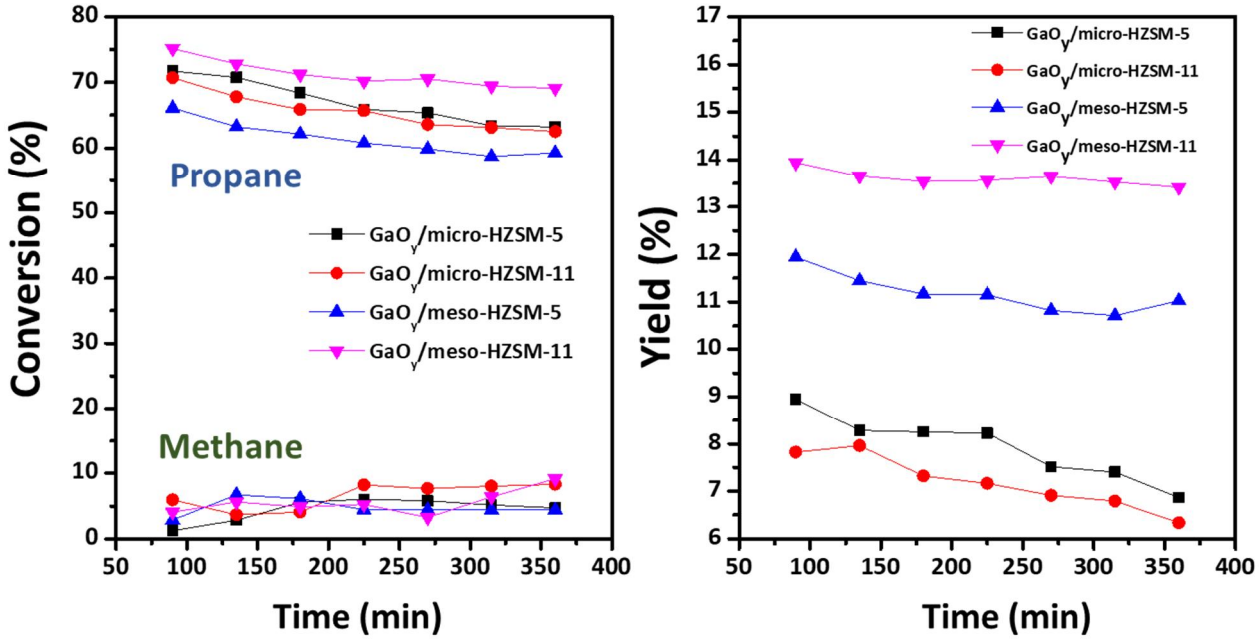

Fig. 4.2.3. Catalytic performance with time on stream over gallium-doped zeolites in the direct dehydroaromatization of methane and propane.

Table 4.2.2. Catalytic performance of gallium-doped zeolite catalysts in the direct dehydroaromatization of methane and propane after a 45-min reaction (reaction temperature = 550 °C, GHSV = 3900 ml/h·g-cat, inert gas ratio (nitrogen:methane:propane) = 7.5:5:0.5)

Catalyst	**GaO_y/micro-HZSM-5**	**GaO_y/meso-HZSM-5**	**GaO_y/micro-HZSM-11**	**GaO_y/meso-HZSM-11**
CH_4 conversion (%)	1.21	2.39	5.92	2.18
C_3H_8 conversion (%)	71.74	72.16	70.74	83.18
Selectivity (%)				
Ethane	8.09	4.71	9.56	2.52
Ethylene	4.56	10.56	2.50	10.16
Propylene	13.59	11.51	16.12	8.30
Butane	0.53	0.13	0.13	0.09
C5	2.09	1.90	1.07	1.62
CO_2	2.01	2.04	2.03	3.27
Aromatics				
Benzene	25.33	28.60	22.11	31.74
Toluene	18.51	20.89	16.18	21.10
Xylene	3.54	4.00	2.88	3.60
Total (%)	78.25	84.35	72.58	82.40

Table 4.2.3. Catalytic performance of gallium-doped zeolite catalysts in the direct dehydroaromatization of methane and propane after a 315-min reaction (reaction temperature = 550 °C, GHSV = 3900 ml/h·g-cat, inert gas ratio (nitrogen:methane:propane) = 7.5:5:0.5)

Catalyst	GaO_y/micro-HZSM-5	GaO_y/meso-HZSM-5	GaO_y/micro-HZSM-11	GaO_y/meso-HZSM-11
CH_4 conversion (%)	4.74	4.39	8.33	6.38
C_3H_8 conversion (%)	63.24	62.56	62.50	72.38
Selectivity (%)				
Ethane	3.11	4.23	4.01	3.47
Ethylene	10.55	10.85	9.23	9.98
Propylene	18.99	15.04	17.96	11.57
Butane	3.09	0.15	2.18	0.11
C5	3.33	2.41	2.75	2.20
CO_2	1.95	2.08	2.01	4.12
Aromatics				
Benzene	19.38	26.44	17.27	27.57
Toluene	15.12	20.86	13.56	22.39
Xylene	3.18	4.39	2.60	4.23
Total (%)	78.7	86.45	69.56	85.64

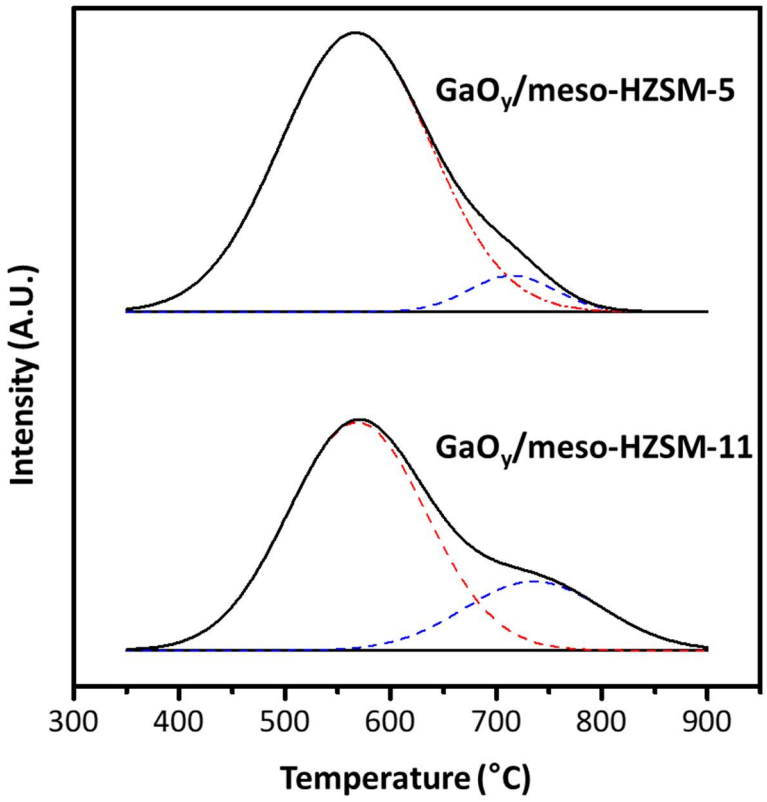

Fig. 4.2.4. H_2-TPR profiles of GaO_y/meso-HZSM-5 and GaO_y/meso-HZSM-11

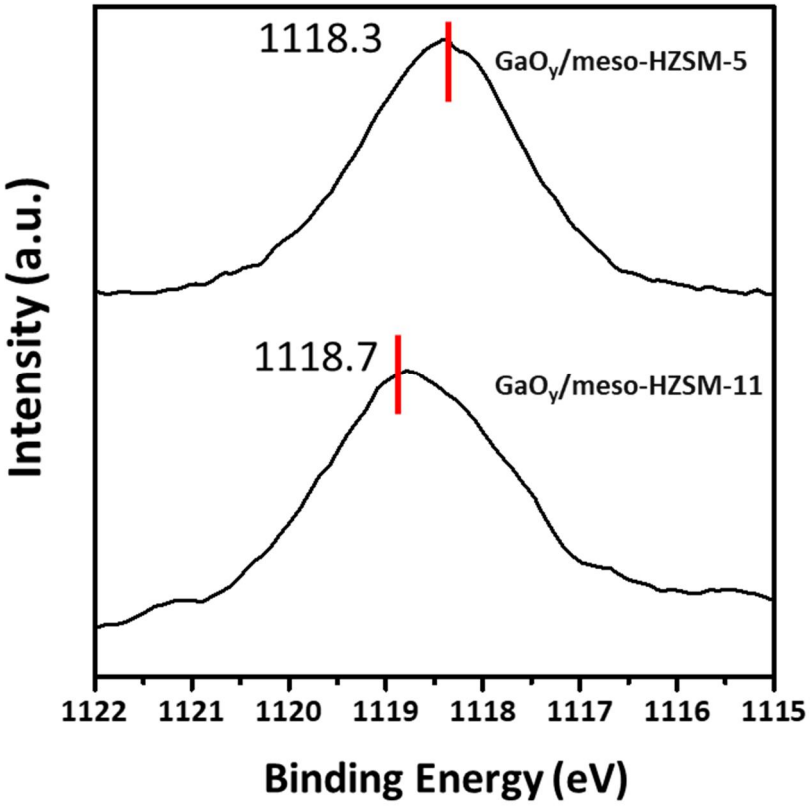

Fig. 4.2.5. Ga $2p_{3/2}$ XPS spectra of GaO_y/meso-HZSM-5 and GaO_y/meso-HZSM-11

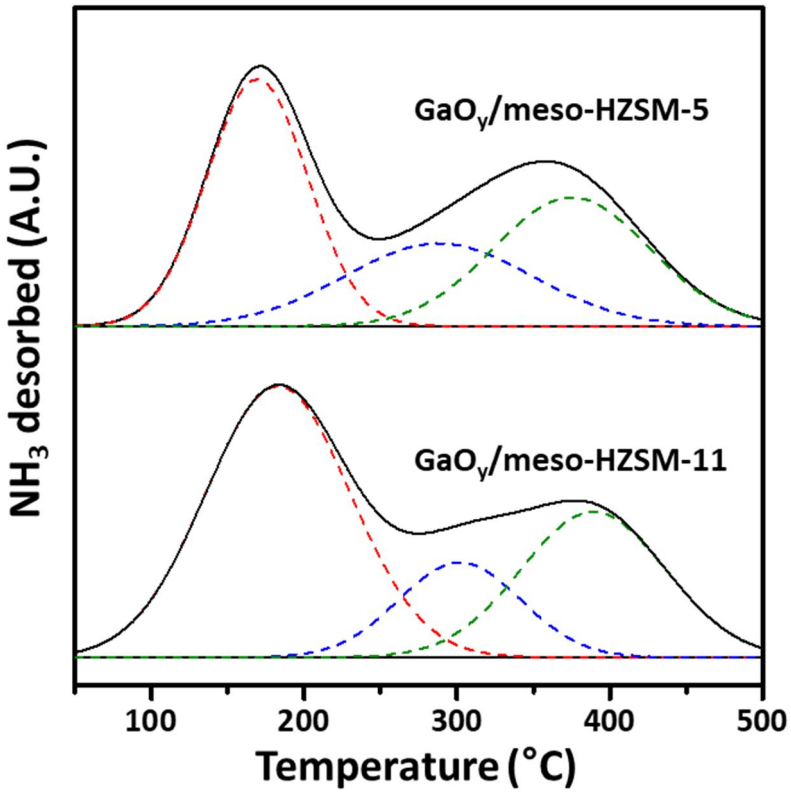

Fig. 4.2.6. NH_3-TPD profiles of GaO_y/meso-HZSM-5 and GaO_y/meso-HZSM-11

Table 4.2.4. Acidity of GaO_y/meso-HZSM-5 and GaO_y/meso-HZSM-11

	Temperature$_{max}$ (°C)			Acidity (mmol/g$_{cat}$)			
Catalyst	**Weak site**	**Medium site**	**Strong site**	**Weak site**	**Medium site**	**Strong site**	**Total acidity**
GaO_y/meso-hzsm-5	169.0	288.1	374.6	0.333 (41.32%)	0.207 (25.65%)	0.267 (33.03%)	0.807
GaO_y/meso-HZSM-11	181.8	310.1	397.8	0.545 (53.45%)	0.246 (24.15%)	0.228 (22.40%)	1.02

4.3. Various amount of gallium loading supported on meso-HZSM-11

4.3.1. Textural properties of $XGaO_y$/meso-HZSM-11 (X = 0, 1, 2, 4 and 8)

As shown in Fig. 4.3.1, textural properties of a series of $XGaO_y$/meso-HZSM-11 (X= 0, 1, 2, 4 and 8) were investigated by nitrogen adsorption-desorption isotherm. The isotherms of a series of $XGaO_y$/meso-HZSM-11 (X= 0, 1, 2, 4 and 8) exhibited type-IV hysteresis loop indicating the maintenance of mesopores in zeolites. In consequence, as the amount of gallium loading increases, surface area of gallium-doped mesoporous zeolites decreases. All calculated surface area are listed in Table 4.3.1.

4.3.2. Catalytic performance of $XGaO_y$/meso-HZSM-11 (X = 0, 1, 2, 4 and 8)

Catalytic performance and conversions of reactants over prepared catalysts were shown in Fig 4.3.2. To be more specific, initial conversion of methane and propane, selectivity to by-product and BTX are listed in Table 4.3.2 (after 45 min. reaction). Conversion and selectivity data after 6 h reaction were also listed in Table 4.3.3 for comparison with initial catalytic performance. It was notable that as weight percent of gallium was greater than 4 (4 wt% and 8 wt%), severe deactivation was found over time. It might be due to aggregation of gallium led to pore blockage of the catalysts. Also, $0GaO_y$/meso-HZSM-11 showed lowest catalytic performance due to lack of Lewis acid site. According to Table 4.3.2, conversion rate of reactant was relatively low compared to other catalysts meaning that reactants were rarely activated by small amount of Lewis

acid site. Among tested catalysts, $1GaO_y$/meso-HZSM-11 exhibited the best catalytic performance without severe deactivation of catalyst. From Table 4.3.2 and Table 4.3.3, loss of carbon balance was not shown while severe loss of carbon were found in case of $0GaO_y$/meso-HZSM-11 and $8GaO_y$/meso-HZSM-11. $0GaO_y$/meso-HZSM-11 had high selectivity to olefins such as ethylene and propylene. Produced olefins can block pores of catalysts over times. As various amount of gallium loading were impregnated, acidic properties of catalysts were also influenced.

4.3.3. Acidic properties of $XGaO_y$/meso-HZSM-11 (X = 0, 1, 2, 4 and 8)

The acidic properties of $XGaO_y$/meso-HZSM-11 (X = 0, 1, 2, 4 and 8) were investigated by NH_3-TPD measurement as shown All calculated acidity is listed in Table 4.3.4. Three peaks of NH_3 desorption for a series of $XGaO_y$/meso-HZSM-11 appeared at different temperatures associated with weak, medium, and strong acid site, respectively. Medium acid site is mainly related to the interaction of extra-framework GaO^+ species with the acidic protons of the zeolite framework. As expected, $0GaO_y$/meso-HZSM-11 contained the lowest amount of Lewis acid site due to lack of gallium metal. The acidity of $1GaO_y$/meso-HZSM-11 was the highest among series of $XGaO_y$/meso-HZSM-11. It was revealed that catalytic performance in dehydroaromatization of methane was directly proportional to total acidity. Also, highest conversion rate of reactants can be elucidated with the amount of strong Lewis acid site as shown in Table 4.3.4. Therefore, $1GaO_y$/meso-HZSM-11 exhibited the best catalytic performance with the largest amount of acidity.

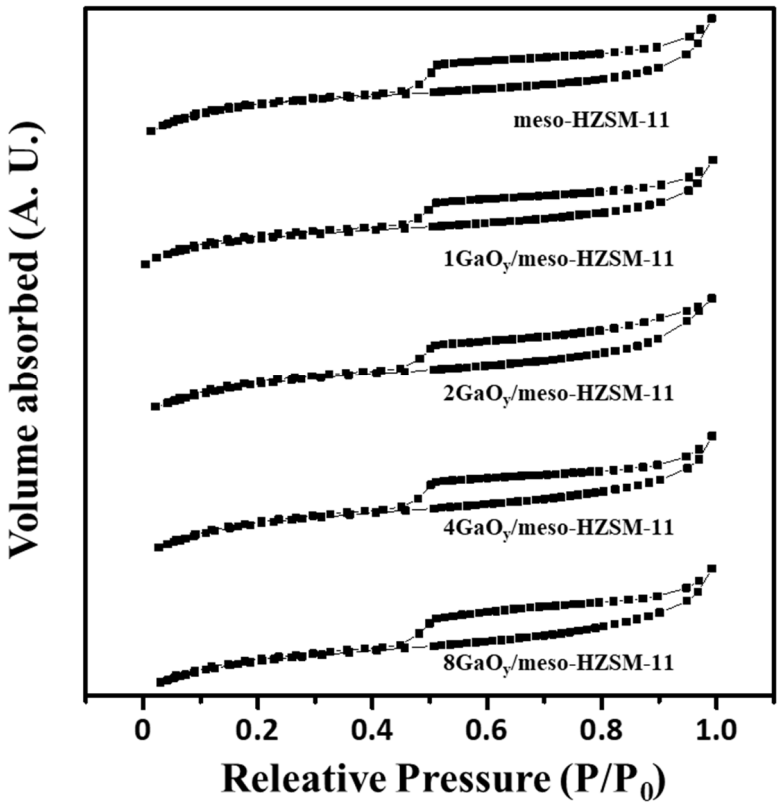

Fig. 4.3.1. Nitrogen adsorption-desorption isotherms of XGaOy/meso-HZSM-11 (X = 0, 1, 2, 4 and 8)

Table 4.3.1. Physicochemical properties of $XGaO_y$/meso-HZSM-11 (X = 0, 1, 2, 4 and 8)

Catalyst	Surface area (m^2/g)[a]
meso-HZSM-11	351.4
1GaO_y/meso-HZSM-11	346.6
2GaO_y/meso-HZSM-11	337.2
4GaO_y/meso-HZSM-11	329.0
8GaO_y/meso-HZSM-11	312.4

[a] Calculated by BET equation

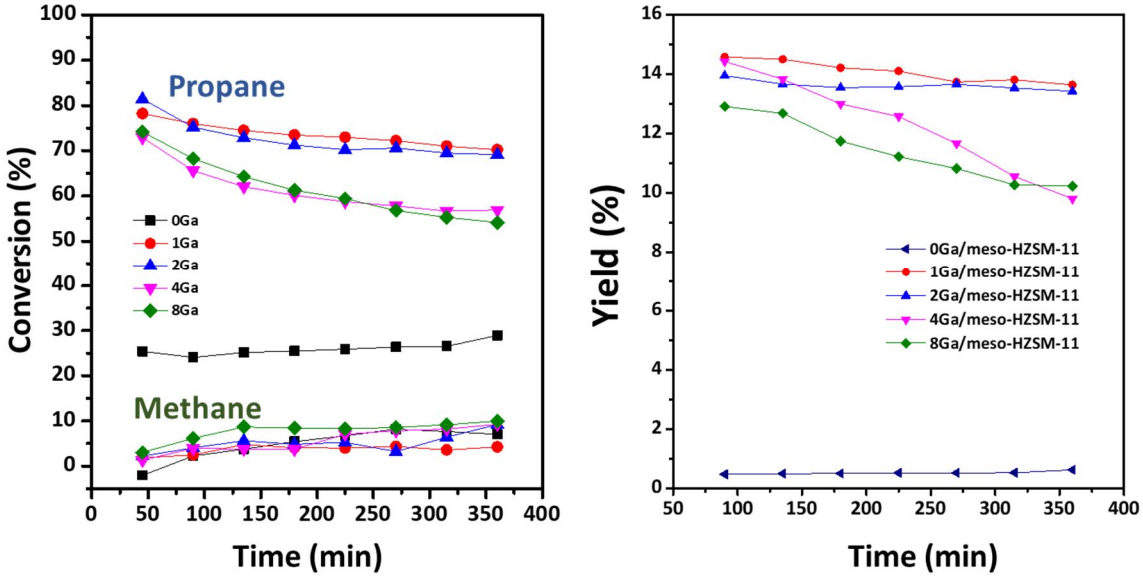

Fig. 4.3.2. Catalytic performance with time on stream $XGaO_y$/meso-HZSM-11 (X = 0, 1, 2, 4 and 8) zeolites in the direct dehydroaromatization of methane and propane.

Table 4.3.2. Catalytic performance of $XGaO_y$/meso-HZSM-11 (X = 0, 1 and 8) zeolite catalysts in the direct dehydroaromatization of methane and propane after a 45-min reaction (reaction temperature = 550 °C, GHSV = 3900 ml/h·g-cat, inert gas ratio (nitrogen:methane:propane) = 7.5:5:0.5)

Catalyst	**$0GaO_y$/meso-HZSM-11**	**$1GaO_y$/meso-HZSM-11**	**$8GaO_y$/meso-HZSM-11**
CH_4 conversion (%)	-2.06	2.03	3.04
C_3H_8 conversion (%)	32.53	80.60	76.65
Selectivity (%)			
Ethane	3.98	1.87	4.61
Ethylene	52.18	11.18	8.93
Propylene	20.30	10.07	9.71
Butane	0.29	0.11	0.12
C5	5.44	1.64	1.87
CO_2	12.80	2.27	1.91
Aromatics			
Benzene	3.44	35.24	29.56
Toluene	1.87	27.35	23.98
Xylene	0.30	4.67	4.46
Total (%)	100.60	94.40	85.15

Table 4.3.3. Catalytic performance of $XGaO_y$/meso-HZSM-11 (X = 0, 1 and 8) zeolite catalysts in the direct dehydroaromatization of methane and propane after a 315-min reaction (reaction temperature = 550 °C, GHSV = 3900 ml/h·g-cat, inert gas ratio (nitrogen:methane:propane) = 7.5:5:0.5)

Catalyst	**$0GaO_y$/meso-HZSM-11**	**$1GaO_y$/meso-HZSM-11**	**$8GaO_y$/meso-HZSM-11**
CH_4 conversion (%)	7.06	3.54	9.13
C_3H_8 conversion (%)	35.72	73.46	59.52
Selectivity (%)			
Ethane	1.91	3.51	5.21
Ethylene	28.12	11.88	8.13
Propylene	11.33	12.91	13.42
Butane	0.16	0.14	0.16
C5	3.18	2.11	2.76
CO_2	7.45	2.77	0.32
Aromatics			
Benzene	2.53	33.44	19.79
Toluene	1.33	26.85	19.25
Xylene	0.215	5.10	3.80
Total (%)	56.23	98.91	74.05

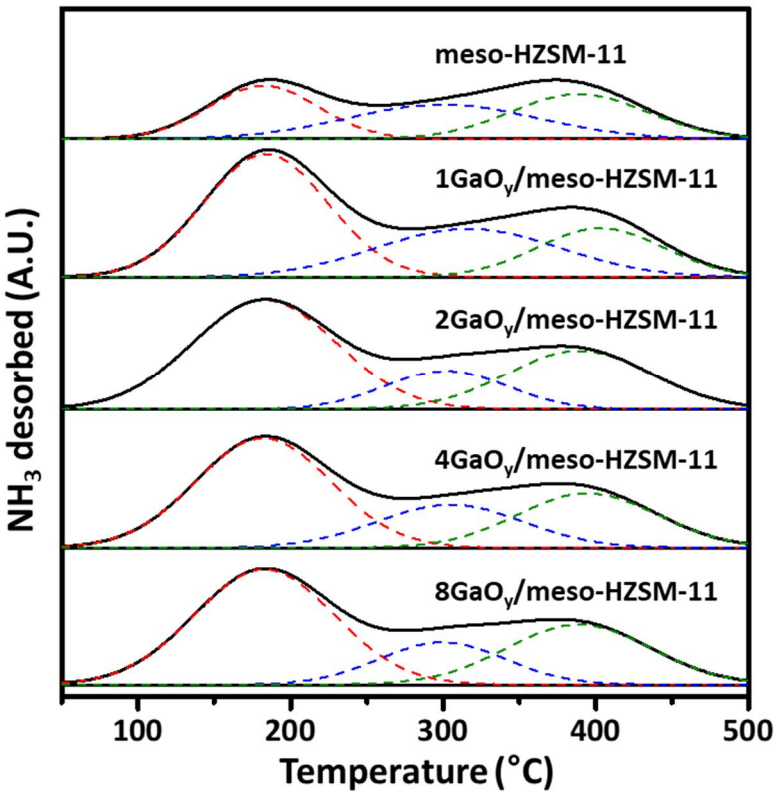

Fig. 4.3.3. NH_3-TPD profiles of $XGaO_y$/meso-HZSM-11 (X = 0, 1, 2, 4 and 8)

Table 4.3.4. Acidity of GaO_y/meso-HZSM-5 and GaO_y/meso-HZSM-11

Catalyst	Temperature$_{max}$ (°C)			Acidity (mmol/g_{cat})			
	Weak site	Medium site	Strong site	Weak site	Medium site	Strong site	Total acidity
meso-HZSM-11	182.2	299.4	388.9	0.256(31.71%)	0.288(35.67%)	0.266(32.93%)	0.807
1GaO$_y$/meso-HZSM-11	183.5	319.1	403.5	0.586(50.11%)	0.366(31.26%)	0.219(18.7%)	1.17
2GaOy/meso-HZSM-11	181.8	310.1	397.8	0.545 (53.45%)	0.246 (24.15%)	0.228 (22.40%)	1.02
4GaOy/meso-HZSM-11	180.9	316.2	401.9	0.455(50.14%)	0.283(31.21%)	0.169(18.65%)	0.908
8GaOy/meso-HZSM-11	181.7	306.7	396.2	0.483(52.41%)	0.227(24.66%)	0.211(22.93%)	0.921

5. Conclusion

In this research, the modification of pore structure of conventional HZSM-5 and HZSM-11 was performed in order to enhance mass transfer and coke resistance of the catalysts. Prepared catalysts were then applied for BTX production by coaromatization of methane and propane. Among transition metal oxides, gallium oxides were doped into prepared catalysts due to advantage of high electron capacity of gallium. Catalytic performance over gallium-doped zeolites were evaluated in the same operation condition. Between gallium-doped conventional HZSM-5 and HZSM-11, HZSM-5 showed better catalytic performance with higher conversion rate of propane. Also, it was found that formation of mesopores enhanced catalytic performance and coke resistance compared to conventional zeolites. According to carbon balance data, gallium-doped microporous zeolites lost relatively large amount of carbon compared to gallium-doped mesoporous zeolites. In case of microporous zeolites, deactivation of catalysts were also found over time. In comparison GaO_y/meso-HZSM-11 with GaO_y/meso-HZSM-5, the effect of introduction of mesopores on HZSM-11 was more dominant than HZSM-5. Higher conversion rate of reactants was corresponding to the interaction between zeolites and highly dispersed gallium species (GaO^+). By H_2-TPR, XPS, and NH_3-TPD, it was revealed the interaction between meso-HZSM-11 and GaO^+ was stronger than the interaction between HZSM-5 and highly dispersed gallium. Not only for the interaction strength, but larger amount of GaO^+ was also measured in GaO_y/meso-HZSM-11. Total acidity of gallium-doped zeolites was also a crucial factor for enhance BTX production. Total acidity of GaO_y/meso-HZSM-11 was greater than that of GaO_y/meso-HZSM-5 as

well.

In order to optimize the acidic properties, various amount of gallium loadings were applied into meso-HZSM-11 denoted as XGaOy/meso-HZSM-11 (X = 0, 1, 2, 4, and 8). Among tested catalysts, $1GaO_y$/meso-HZSM-11 showed the best catalytic performance with largest amount of acidity. It was also notable that $4GaO_y$/meso-HZSM-11 and $8GaO_y$/meso-HZSM-11 showed severe deactivation over reaction time due to pore blockage with aggregation of gallium species. In this work, it was revealed that the interaction between gallium species and zeolites played an important role on activating reactants by hydrogen transfer. Total acidity (weak Lewis acidity + strong Lewis acidity + Brönsted acidity) of the catalysts exhibited a volcano-shaped trend with respect to gallium oxide loading. Initial conversion of methane and propane together with BTX yield also showed volcano-shaped trends with respect to gallium oxide loading. Thus, total acidity of the catalysts was correlated to the catalytic performance in the BTX production by coaromatization of methane and propane.

Bibliography

[1] M.Y. Gim, C. Song, T.H. Kim, J.H. Song, D.H. Kim, K.-Y. Lee, I.K. Song, "BTX production by coaromatization of methane and propane over gallium oxide supported on mesoporous HZSM-5", Mol. Catal., 439 (2017) 134-142.

[2] L. Chen, L. Lin, Z. Xu, X. Li, T. Zhang, "Dehydro-oligomerization of Methane and Ethylene and Aromatics over Molybdenum/HZSM-5 Catalyst", J. Catal. 157, 190-200.

[3] Y. Xu, X. Bao, L. Lin," Direct conversion of methane under nonoxidative conditions", J.Catal., 216 (2003) 386-395.

[4] A. Sridhar, M. Rahman, S.J. Khatib, "Enhancement of Molybdenum/ZSM-5 Catalysts in Methane Aromatization by the Addition of Iron Promoters and by Reduction/Carburization Pretreatment", ChemCatChem, (2018).

[5] X. Su, G. Wang, X. Bai, W. Wu, L. Xiao, Y. Fang, J. Zhang, "Synthesis of nanosized HZSM-5 zeolites isomorphously substituted by gallium and their catalytic performance in the aromatization", Chem. Eng. J., 293 (2016) 365-375.

[6] W. Wannapakdee, C. Wattanakit, V. Paluka, T. Yutthalekha, J. Limtrakul, "One-pot synthesis of novel hierarchical bifunctional Ga/HZSM-5 nanosheets for propane aromatization", RSC Adv., 6 (2016) 2875-2881.

[7] Y. Fang, X. Su, X. Bai, W. Wu, G. Wang, L. Xiao, A. Yu, "Aromatization over nanosized Ga-containing ZSM-5 zeolites prepared by different methods: Effect of acidity of active Ga species on the catalytic performance", J. Ener.Chem., 26 (2017) 768-775.

[8] W.-g. Kim, J. So, S.-W. Choi, Y. Liu, R.S. Dixit, C. Sievers, D.S. Sholl, S. Nair, C.W. Jones, "Hierarchical Ga-MFI Catalysts for Propane Dehydrogenation", Chem. Mater., 29 (2017) 7213-7222.

[9] .S. Phatanasri, P. Praserthdam, A. Sripusitto, "Aromatization of light paraffins over Ga-containing MFI-type Catalyst" Korean. J. Chem. Eng. 17 (40, 409-413

[10] P. He, J. Jarvis, S. Meng, A. Wang, S. Kou, R. Gatip, M. Yung, L. Liu, H. Song, "Co-aromatization of methane with olefins: The role of inner pore and external surface catalytic sites", Appl. Catal. B: Enviro., 234 (2018) 234-246.

[11] J. Zhou, Z. Hua, J. Shi, Q. He, L. Guo, M. Ruan, "Synthesis of a hierarchical micro/mesoporous structure by steam-assisted post-crystallization", Chemistry, 15 (2009) 12949-12954.

[12] J. Zhou, Z. Hua, X. Cui, Z. Ye, F. Cui, J. Shi, "Hierarchical mesoporous TS-1 zeolite: a highly active and extraordinarily stable catalyst for the selective oxidation of 2,3,6-trimethylphenol", Chem Commun (Camb), 46 (2010) 4994-4996.

[13] J. Zhou, Z. Hua, Z. Liu, W. Wu, Y. Zhu, J. Shi, "Direct Synthetic Strategy of Mesoporous ZSM-5 Zeolites by Using Conventional Block Copolymer Templates and the Improved Catalytic Properties", ACS Catal., 1 (2011) 287-291.

[14] J. Guo, H. Lou, X. Zheng, "Energy-Efficient coaromatization of methane and propane", J. Nat. Gas Chem., 18 (2009) 260-272.

[15] L. Zhang, H. Liu, X. Li, S. Xie, Y. Wang, W. Xin, S. Liu, L. Xu, "Differences between ZSM-5 and ZSM-11 zeolite catalysts in 1-hexene aromatization and isomerization", Fuel Processing Technology, 91 (2010) 449-455.

[16] Q. Yu, C. Cui, Q. Zhang, J. Chen, Y. Li, J. Sun, C. Li, Q. Cui, C. Yang, H. Shan,

"Hierarchical ZSM-11 with intergrowth structures: Synthesis, characterization and catalytic properties", J.Ener. Chem., 22 (2013) 761-768.

[17] M.V. Luzgin, A.V. Toktarev, V.N. Parmon, A.G. Stepanov, "Coaromatization of Methane with Propane on Mo-Containing Zeolite H-BEA: A Solid-State NMR and GC-MS Study", J. Phys. Chem. C, 117 (2013) 22867-22873.

[18] S. Majhi, P. Mohanty, H. Wang, K.K. Pant, "Direct conversion of natural gas to higher hydrocarbons: A review", J. Ener. Chem., 22 (2013) 543-554.

[19] A. Bhan, W. Nicholas Delgass, "Propane Aromatization over HZSM-5 and Ga/HZSM-5 Catalysts", Catal. Rev., 50 (2008) 19-151.

[20] H. Xiao, J. Zhang, X. Wang, Q. Zhang, H. Xie, Y. Han, Y. Tan, "A highly efficient Ga/ZSM-5 catalyst prepared by formic acid impregnation and in situ treatment for propane aromatization", Catal. Sci.& Tech., 5 (2015) 4081-4090.

초 록

최근 메탄과 경유 파라핀으로 구성된 셰일 가스 (shale gas)의 개발로 메탄과 경유 파라핀의 효율적인 전환에 대한 많은 연구가 시도 되고 있다. 그 중에서도 수요가 급증하고 있는 BTX의 생산에 관한 연구가 주목 받고 있다. 본 연구에서는 메탄과 프로판의 직접 탈수소방향족화로 BTX (벤젠, 톨루엔 및 자일렌) 제조를 위해 제올라이트의 기공 구조의 변형을 연구하고 적용하였다. 특히, 중형기공 형성을 위해서 탄소 주형물질인 BP-2000을 기존 미세기공성 HZSM-5 및 HZSM-11에 도입하였다. 중형기공성 HZSM-5 및 HZSM-11은 기존 제올라이트의 물질 전달 및 코크 저항성을 향상시키기 위해 연구에 도입되었고 제조되었다. 반응물인 메탄과 프로판을 활성화시키기 위해서 상기에 제조된 중형기공성 제올라이트 및 미세기공 제올라이트에 동일한 양의 갈륨 (각 제올라이트에 대해 2 중량 %)에 습윤함침법을 사용하여 도입하였다. 갈륨 산화물이 담지된 중형기공성 제올라이트는 코크의 축척양이 미세기공성 제올라이트 보다 낮았고 중형기공성 제올라이트가 미세기공성 제올라이트 보다 높은 BTX 선택성 및 BTX 수율을 보였다. GaO_y/meso-HZSM-5와 GaO_y/meso-HZSM-11 사이에서는 meso-HZSM-11에 중형기공을 도입 할 때 meso-HZSM-5보다 효과가 더 뛰어났다. 제올라이트와 GaO^+ 종 사이의 상호작용은 탈수소방향족화의 속도 결정 단계인 반응물의 탈수소화에 중요한

역할을 하는 것으로 알려졌다. XPS, H_2-TPR 및 NH_3-TPD 분석에 따르면, GaO_y/meso-HZSM-11은 GaO_y/meso-HZSM-5 보다 GaO^+ 종과 강한 상호 작용을 보였으며, GaO_y/meso-HZSM-11에서 GaO^+ 종이 보다 많은 양이 관찰되었고, 이는 메탄과 프로판의 높은 전환율에 영향을 끼치는 것을 발견하였다.

따라서 촉매 성능을 최적화하기 위해 다양한 양의 갈륨 산화물 부하량 (X, wt %)을 갖는 일련의 $XGaO_y$/meso-HZSM-11 (X = 0, 1, 2, 4 및 8) $XGaO_y$/meso-HZSM-11의 산 성질과 촉매 성능 사이의 상관 관계를 조사 하였다. 테스트 한 촉매 중 $1GaO_y$/meso-HZSM-11은 가장 높은 산성도를 가지며 최고의 촉매 성능을 보였다. 또한, $4GaO_y$/meso-HZSM-11 및 $8GaO_y$/meso-HZSM-11은 갈륨의 로딩양이 적은 촉매에 비해서 시간 경과에 따라 심각한 촉매 비활성화를 보였다. 따라서, 메탄과 프로판의 동시 방향족 화에 의해 BTX 생성을 개선시키기 위해서는 갈륨 로딩의 최적량이 요구되는 것을 발견하였다.

주요어 : BTX, 갈륨 산화물, 중형기공성 HZSM-5, 중형기공성 HZSM-11, 동시 방향족화, 탈수소방향족화, 메탄, 프로판

학번 : 2016-25837